applied optics

Analytical solution of the correlation transport equation with static background: beyond diffuse correlation spectroscopy

Tiziano Binzoni,[1,2,*] André Liemert,[3] Alwin Kienle,[3] and Fabrizio Martelli[4]

[1]Département de Neurosciences Fondamentales, University of Geneva, Geneva, Switzerland
[2]Département de l'Imagerie et des Sciences de l'Information Médicale, University Hospital, Geneva, Switzerland
[3]Institut für Lasertechnologien in der Medizin und Meßtechnik, Helmholtzstraße 12, D-89081 Ulm, Germany
[4]Dipartimento di Fisica e Astronomia dell'Università degli Studi di Firenze, Sesto Fiorentino, Firenze, Italy
*Corresponding author: tiziano.binzoni@unige.ch

Received 26 July 2016; revised 7 September 2016; accepted 18 September 2016; posted 19 September 2016 (Doc. ID 272427); published 17 October 2016

The correlation transport equation (CTE) is the natural generalization of the theory for diffusion correlation spectroscopy and represents a more precise model when dealing with measurements of particle movement in fluids or red blood cell flow in biological tissues. Unfortunately, the CTE is not methodically used due to the complexity of finding solutions. It is shown that actually a very simple modification of the theory/software for the solution of the radiative transport equation allows one to obtain exact solutions of the CTE. The presence of a static background is also taken into account and its influence on the CTE solutions is discussed. The proposed approach permits one to easily work beyond the diffusion regime and potentially for any optical and/or physiological value. The validity of the approach is demonstrated by using "gold standard" Monte Carlo simulations.

OCIS codes: (170.0170) Medical optics and biotechnology; (170.3660) Light propagation in tissues; (170.3340) Laser Doppler velocimetry; (290.5825) Scattering theory.

http://dx.doi.org/10.1364/AO.55.008500

1. INTRODUCTION

The measurement of temporal autocorrelation functions has represented for a considerable amount of time one of the approaches that permits the assessment of moving particle properties in fluid media (e.g., particle diameter, fluid viscosity, diffusion constant) such as gels or paint [1]. The general theory behind this method is based on the correlation transfer equation (CTE) [1,2]. In fact, the CTE allows one to obtain the electric field autocorrelation function, $G_1(\mathbf{r}, \tau)$, exploited to build a model for the experimental data, from which the moving particle properties are derived.

In biomedical optics, one of the interesting byproducts generated by the study of the CTE is represented by a technique named diffuse correlation spectroscopy (DCS). DCS is a noninvasive optical method allowing the monitoring of blood flow in human tissues [3–6]. In practice, DCS theory is obtained by considering a first-order approximation of the original CTE [4,7]. For this reason, also at the heart of DCS, there is the problem of the exact definition of $G_1(\mathbf{r}, \tau)$ [4], where $\mathbf{r} = (x, y, z)$ represents the spatial position in Cartesian coordinates, and τ the correlation time. The function $G_1(\mathbf{r}, \tau)$ is at the basis of the algorithms that allow us to assess, for example, tissue blood flow in human tissues. Thus, precise knowledge of $G_1(\mathbf{r}, \tau)$, together with the knowledge of its dependence on optical and physiological parameters, is fundamental for a better understanding of the DCS theory and for improving the reliability of DCS instrumentation. The use of DCS instrumentation may one day be exploited for patient monitoring, where inappropriate blood flow data generation might have serious consequences for the patient's health.

Nowadays, while CTE can in principle generate suitable $G_1(\mathbf{r}, \tau)$, in the biomedical optics practice $G_1(\mathbf{r}, \tau)$ still remain an approximated solution of the CTE (diffusion approximation). This approximation may represent a practical limit, for example, beyond the diffusion regime or for some particular optical or physiological values [8]. The absence of the methodical use of CTE in biomedical optics, and in general when dealing with moving particle properties in fluids, is probably due to the mathematical complexity of finding CTE solutions.

The aim of the present contribution is to propose a simple method allowing us to solve the CTE, a method based on the already well-tested theory of photon transport in random media. As far as we know, this is the first analytical solution of the CTE. It will be shown that a simple mathematical modification of the analytical theory/software for the radiative transport equation (RTE) allows one to easily obtain exact CTE solutions

and thus reliable $G_1(\mathbf{r},\tau)$ values. Moreover, it will be shown that this modification is also able to account for the presence of a static background in the medium (nonmoving scatterers). This is extremely important for some human tissues, such as the bone, where the moving scatterers concentration (red blood cells) is very low compared to the static tissue scatterers. In fact, this may invalidate the DCS theory [9]. The proposed approach and results are tested by using the "gold standard" Monte Carlo (MC) simulations.

2. METHODS

In the first part of this section, the CTE is presented. Then, the CTE solution method is described and applied to the tutorial case of an homogeneous semi-infinite medium, containing moving scatterers in a static background, with a unitary isotropic emitting point light source. The solution is given for any source–detector distance ρ and correlation time τ. A Brownian distribution for the moving particles'/scatterers' speed has been chosen.

In the second part of this section, the reference MC method is explained. The "gold standard" MC data will be used in Section 3 to prove the reliability of the proposed CTE solution.

A. Solution of the Correlation Transport Equation

1. General CTE

It is well known [1,2,10,11] that the general expression for the unnormalized directional and temporal field autocorrelation function, $G_1(\mathbf{r},\hat{\Omega},t,\tau)$, is

$$\left[\frac{1}{v}\frac{\partial}{\partial t}+\hat{\Omega}\cdot\nabla_{\mathbf{r}}+\mu_t\right]G_1(\mathbf{r},\hat{\Omega},t,\tau)$$
$$=\mu_s\int g_{1,\text{single}}(\hat{\Omega},\hat{\Omega}',\tau)f(\hat{\Omega},\hat{\Omega}')G_1(\mathbf{r},\hat{\Omega}',t,\tau)\mathrm{d}\hat{\Omega}'+S(\mathbf{r},\hat{\Omega},t), \quad (1)$$

where μ_s is the scattering coefficient; $\mu_t=\mu_s+\mu_a$ the total extinction or attenuation coefficient, with μ_a representing the absorption coefficient; v is the speed of light in the medium; t the time, and τ the correlation time. Note that, when finding the analytical solution of Eq. (1), τ may be intuitively seen as any t-independent parameter such as μ_s or μ_a. The unit vector $\hat{\Omega}'$ describes the direction of a photon before the interaction with a moving scatterer and $\hat{\Omega}$ the direction after the interaction. The notation $\hat{\Omega}\cdot\nabla_{\mathbf{r}}$ represents the scalar product between $\hat{\Omega}$ and the gradient operator. The function $f(\hat{\Omega},\hat{\Omega}')$ is the phase function and $g_{1,\text{single}}(\hat{\Omega},\hat{\Omega}',\tau)$ is the normalized field autocorrelation function for a single scattering event with a moving scatterer. The function $S(\mathbf{r},\hat{\Omega},t)$ describes a t-dependent light source intensity. Equation (1) holds in the case when all the scatterers are moving. In presence of a static background, with a probability $P_m\in[0,1]$ that a scatterer is a moving scatterer, Eq. (1) must be slightly modified as

$$\left[\frac{1}{v}\frac{\partial}{\partial t}+\hat{\Omega}\cdot\nabla_{\mathbf{r}}+\mu_t\right]G_1(\mathbf{r},\hat{\Omega},t,\tau)$$
$$=\mu_sP_m\int g_{1,\text{single}}(\hat{\Omega},\hat{\Omega}',\tau)f(\hat{\Omega},\hat{\Omega}')G_1(\mathbf{r},\hat{\Omega}',t,\tau)\mathrm{d}\hat{\Omega}'$$
$$+\mu_s(1-P_m)\int f(\hat{\Omega},\hat{\Omega}')G_1(\mathbf{r},\hat{\Omega}',t,\tau)\mathrm{d}\hat{\Omega}'+S(\mathbf{r},\hat{\Omega},t), \quad (2)$$

where in the new term the dynamic function $g_{1,\text{single}}(\hat{\Omega},\hat{\Omega}',\tau)$ does not appear, because this term is taken into account only for the static component as in a normal RTE. From Eq. (2), the unnormalized temporal field autocorrelation function, $G_1(\mathbf{r},t,\tau)$, is obtained as

$$G_1(\mathbf{r},t,\tau)=\int_{\Omega_d}(\hat{\Omega}\cdot\hat{\mathbf{n}})G_1(\mathbf{r},\hat{\Omega},t,\tau)\mathrm{d}\hat{\Omega}, \quad (3)$$

where Ω_d is the acceptance solid angle of the "detection" system. It is worth noting that experimentally, in biomedical optics, the measured variable is not $G_1(\mathbf{r},t,\tau)$ but the intensity autorrelation function $G_2(\mathbf{r},t,\tau)$. The theoretical function $G_1(\mathbf{r},t,\tau)$ is actually used to derive an analytical model for $G_2(\mathbf{r},t,\tau)$. Then, the $G_2(\mathbf{r},t,\tau)$ model is used to fit the $G_2(\mathbf{r},t,\tau)$ experimental data and to derive the parameters of interest (e.g., blood flow). For this reason, it is mandatory that $G_1(\mathbf{r},t,\tau)$ and $G_2(\mathbf{r},t,\tau)$ are, respectively, computed/measured over the *same* solid angle Ω_d by taking into account the *same* experimental geometry.

In summary, Eqs. (2) and (3) describe $G_1(\mathbf{r},t,\tau)$ when a fraction of the scatterers in the investigated medium are moving. The special case $P_m=0$ gives the classical RTE (no moving scatterers) and $P_m=1$ gives Eq. (1) (no static background).

2. CTE for the Determination of "Flow"

When considering the CTE for the determination of tissue blood flow (perfusion) or, in general, particle movement in fluids, Eq. (2) can be slightly simplified. In fact, in this case $S(\mathbf{r},\hat{\Omega},t)$ becomes t-independent because the utilized light source is usually a constant intensity CW laser. This implies that the time derivative on the left hand side of Eq. (1) is nil. Moreover, the function $f(\hat{\Omega},\hat{\Omega}')$ is considered to be a function only of the scattering angle existing between $\hat{\Omega}$ and $\hat{\Omega}'$. This means that $f(\hat{\Omega},\hat{\Omega}')$ can be formally expressed as $f(\hat{\Omega}\cdot\hat{\Omega}')$ (where $\hat{\Omega}\cdot\hat{\Omega}'$ is the scalar product). For the typical scattering speed distributions usually adopted, e.g., in biomedical optics or other applications considered in the frame of scatterer movement assessment (see below), $g_{1,\text{single}}(\hat{\Omega},\hat{\Omega}',\tau)$ can also be considered to depend only on $\hat{\Omega}\cdot\hat{\Omega}'$.

For the above reasons, Eq. (2), for a unitary isotropic-emitting point light source of 1 W mm^{-3} sr^{-1}, may be written as

$$[\hat{\Omega}\cdot\nabla_{\mathbf{r}}+\mu_t]G_1(\mathbf{r},\hat{\Omega},\tau)$$
$$=\mu_sP_m\int g_{1,\text{single}}(\hat{\Omega}\cdot\hat{\Omega}',\tau)f(\hat{\Omega}\cdot\hat{\Omega}')G_1(\mathbf{r},\hat{\Omega}',\tau)\mathrm{d}\hat{\Omega}'$$
$$+\mu_s(1-P_m)\int f(\hat{\Omega}\cdot\hat{\Omega}')G_1(\mathbf{r},\hat{\Omega}',\tau)\mathrm{d}\hat{\Omega}'$$
$$+\frac{S_0\delta(x)\delta(y)\delta(z-z_0)}{4\pi}, \quad (4)$$

where $S_0=1$ W, $\delta(.)$ is the Dirac function, and z_0 is the position of the light source on the z axis, i.e., $(0,0,z_0)$. The t-dependence of $G_1(\mathbf{r},\hat{\Omega},t,\tau)$ has disappeared and thus the notation $G_1(\mathbf{r},\hat{\Omega},\tau)$ is used. The terms appearing in Eq. (4) have the following units: $G_1(\mathbf{r},\hat{\Omega},\tau)$: W mm^{-2} sr^{-1}; $\hat{\Omega}\cdot\nabla_{\mathbf{r}}$, μ_t and μ_s: mm^{-1}; P_m and $g_{1,\text{single}}(\hat{\Omega}\cdot\hat{\Omega}',\tau)$: no units; $f(\hat{\Omega}\cdot\hat{\Omega}')$: sr^{-1}; and $\mathrm{d}\hat{\Omega}'$: sr. The detector is situated at a distance $\rho=(x^2+y^2)^{1/2}$ from the origin of the axes.

For the explanatory purposes of the present contribution, we will consider a semi-infinite medium and a reflectance detection scheme. Thus, in this case, Eq. (3) becomes

$$G_1(\mathbf{r},\tau)=\int_{\hat{\Omega}\cdot\hat{\mathbf{n}}>0}(\hat{\Omega}\cdot\hat{\mathbf{n}})G_1(\mathbf{r},\hat{\Omega},\tau)\mathrm{d}\hat{\Omega}, \tag{5}$$

where the integral is evaluated at $\mathbf{r}=(x,y,z=0)$ and $\|\mathbf{r}\|=\rho$, and where $\hat{\mathbf{n}}=-\hat{\mathbf{z}}$ is the corresponding outward unit vector normal to the semi-infinite medium surface. The function $f(\hat{\Omega}\cdot\hat{\Omega}')$ is modeled with the classical Henyey–Greenstein function [12], largely utilized in biomedical optics. The $g_{1,\mathrm{single}}(\hat{\Omega}\cdot\hat{\Omega}',\tau)$ for moving scatterers with Brownian motion is [10,11]

$$g_{1,\mathrm{single}}(\hat{\Omega}\cdot\hat{\Omega}',\tau)=e^{-2D_\mathrm{B}k^2(1-\hat{\Omega}\cdot\hat{\Omega}')\tau}, \tag{6}$$

where D_B is the Brownian diffusion coefficient and $k=2\pi n/\lambda$, where n is the refractive index of the medium and λ is the wavelength of the laser light source.

3. Relationship between CTE and RTE

To solve Eq. (4), let us first define the new function,

$$F(\hat{\Omega}\cdot\hat{\Omega}',\tau)=\{[g_{1,\mathrm{single}}(\hat{\Omega}\cdot\hat{\Omega}',\tau)-1]P_\mathrm{m}+1\}f(\hat{\Omega}\cdot\hat{\Omega}'). \tag{7}$$

By substituting Eq. (7) in Eq. (1) we obtain

$$[\hat{\Omega}\cdot\nabla_\mathbf{r}+\mu_\mathrm{t}]G_1(\mathbf{r},\hat{\Omega},\tau)=\mu_\mathrm{s}\int F(\hat{\Omega}\cdot\hat{\Omega}',\tau)G_1(\mathbf{r},\hat{\Omega}',\tau)\mathrm{d}\hat{\Omega}'+\frac{S_0\delta(x)\delta(y)\delta(z-z_0)}{4\pi}. \tag{8}$$

We immediately see that Eq. (8) is the classical RTE. This means that all the known mathematical tools utilized to solve the RTE can be directly applied to solve Eq. (8). The only difference is that the phase function $f(\hat{\Omega}\cdot\hat{\Omega}')$, found in the RTE, is now replaced by $F(\hat{\Omega}\cdot\hat{\Omega}')$. Considering that the solution of the RTE, and the related software, for a semi-infinite medium, has already been developed and explained elsewhere [13–17], we report here the only point differing from the original approach. This point represents, at the same time, the mathematical "simple trick" allowing us to solve Eq. (8).

In the original RTE solution, $f(\hat{\Omega}\cdot\hat{\Omega}')$ is expressed in terms of rotated spherical harmonics (see Eq. (9) in Ref. [16]). This can be done because $\hat{\Omega}\cdot\hat{\Omega}'\in[-1,1]$. Considering that $F(\hat{\Omega}\cdot\hat{\Omega}',\tau)$ satisfies the same mathematical conditions, we can similarly write

$$F(\hat{\Omega}\cdot\hat{\Omega}',\tau)=\sum_{l=0}^{P_N}\sum_{M=-l}^{l}F_l(\tau)Y_{lM}(\hat{\Omega};\hat{\mathbf{k}})Y_{lM}^*(\hat{\Omega}';\hat{\mathbf{k}}), \tag{9}$$

where $Y_{lM}(\hat{\Omega};\hat{\mathbf{k}})$ are the rotated spherical harmonics around the unit vector $\hat{k}$. The parameter P_N is an odd positive integer and it depends on the so-called chosen "P_N" approximation when the algorithm is implemented.

Note that $f(\hat{\Omega}\cdot\hat{\Omega}')$ represents just the particular case: $F(\hat{\Omega}\cdot\hat{\Omega}',\tau=0)=f(\hat{\Omega}\cdot\hat{\Omega}')$. The expansion coefficients $F_l(\tau)$ in Eq. (9) are defined as

$$F_l(\tau)=2\pi\int_{-1}^{1}F(\zeta,\tau)P_l(\zeta)\mathrm{d}\zeta, \tag{10}$$

where $P_l(\zeta)$ are the Legendre polynomials. Again, we have the particular case $F_l(\tau=0)=f_l$, where f_l are the expansion coefficients for $f(\hat{\Omega}\cdot\hat{\Omega}')$ appearing in Eq. (9) of Ref. [16]. Thus, in practice, it is sufficient to substitute in the original RTE solution the expansion coefficients f_l with $F_l(\tau)$, i.e.,

$$f_l\xrightarrow{\text{replaced by}}F_l(\tau), \tag{11}$$

to obtain the solution of Eqs. (8) and (3). Therefore, the wanted $G_1(\mathbf{r},\tau)$ can be computed by setting $\mathbf{r}$ to the detector position, i.e., at $z=0$ and at distance ρ from the origin. Due to the cylindrical symmetry of the problem, we will formally express this from now on as $G_1(\rho,\tau)$. One calculation must be performed for each desired τ value. No other changes are necessary to be introduced in the RTE software or theory.

An important technical point concerning Eq. (10) deserves our attention. To obtain the $F_l(\tau)$ values, Eq. (10) is first integrated analytically $\forall\ l\in\mathbb{N}$. Then, the analytical solution is used to assess the numerical $F_l(\tau)$ values. This procedure improves the precision of the final numerical calculation allowing to us obtain $F_l(\tau)$. However, it must be noted that the latter numerical procedure must be performed with a high number of digits of precision. Precision given, e.g., by standard programming languages with 64-bit numbers is not enough to produce reliable results for F_l (results not shown). For this reason the software utilized to generate F_l was written in MATLAB language in combination with the suitable toolboxes allowing us to work with variable-precision arithmetic.

In practice, the RTE software utilized to implement the proposed analytical CTE solution was the one proposed in Ref. [16]. The isotropic-emitting point light source was set at

$$z_0=(\mu_\mathrm{a}+(1-g)\mu_\mathrm{s})^{-1}, \tag{12}$$

where g is the known mean cosine of the angle between $\hat{\Omega}$ and $\hat{\Omega}'$, classically appearing in the Henyey–Greenstein function $f(\hat{\Omega}\cdot\hat{\Omega}')$. The CTE solution has been implemented for the approximation orders $P_N=\{1,3,5,7,11,13\}$ [16].

B. CTE Solution on a Ring (Detector)

The detector of a reference MC simulation cannot be infinitely thin, as may be the case for an analytical solution. For this reason an annulus detector, compatible with the MC method, has also been considered for the CTE solution. Thus, the $G_1(\rho,\tau)$ solution for the annulus, $\overline{G}_1(\rho,\tau)$, can be obtained as

$$\overline{G}_1(\rho,\tau)=\frac{1}{S}\sum_{i=1}^{N_\mathrm{r}}G_1(\rho_i,\tau)s_i, \tag{13}$$

where S is the surface of the annulus and ρ its mean radius (mean between maximum and minimum radius of the annulus). The annulus has been subdivided in N_r concentric annuli with mean radius ρ_i and surface s_i (i.e., $\sum_i s_i=S$ and $\rho_{i+1}-\rho_i=$ constant). If $S\to 0$ then $\overline{G}_1(\rho,\tau)=G_1(\rho,\tau)$.

C. Monte Carlo Code

The MC code used to test the CTE solution has been written by following the procedure proposed in Ref. [11]. As explained in Ref. [11], the advantage of this code is that it can potentially solve the general Eq. (1), without making unwanted assumptions, such as the ones introduced in previous theories [18–20], i.e., small τ; the average angle $\langle\|\hat{\Omega}-\hat{\Omega}'\|^2\rangle\sim 2(1-g)$; or mean scattering events on a path of length s approximated to s/μ_s. In fact, these assumptions do not allow the representation of an

exact equivalent MC model for the CTE and are mainly linked to a diffusion regime. To exactly simulate the same physical system as the one described by the analytical CTE, the position of the isotropic light source was set to $(0, 0, z_0)$ [Eq. (12)]. The refractive index of air was set to 1. Simulations have been performed on a computer cluster with 12 nodes. For each MC simulation (i.e., one $\overline{G}_1(\rho, \tau)$ curve) 10^7 photon packets have been generated. To obtain an estimation of the standard deviation, the same MC simulation has been repeated 5 times.

In practice, the MC uses a classical scheme to compute the reflectance on a semi-infinite medium with fixed particles, but where the photon weight of a given detected photon packet is multiplied by an exponential correlation function

$$E(\tau) = \prod_{i=1}^{n_{\text{scatt}}} e^{-2D_B k^2 (1-\hat{\Omega}_i \cdot \hat{\Omega}'_i)\tau}, \quad \textbf{(14)}$$

where $\hat{\Omega}_i$ and $\hat{\Omega}'_i$ are $\hat{\Omega}$ and $\hat{\Omega}'$ at the ith scattering event with a *moving* scatterer, and n_{scatt} the number of (*moving*) scattering events on the considered photon path. The product $\hat{\Omega}_i \cdot \hat{\Omega}'_i$ is the cosine of the angle between $\hat{\Omega}_i$ and $\hat{\Omega}'_i$ at the ith scattering event with a moving scatterer. To decide if a scatterer is moving or not, a random number $\chi \in [0, 1]$ uniformly distributed is chosen, then if $\chi \leq P_{\text{m}}$, the scatterer is moving. This procedure allows us to compute the MC test data for $\overline{G}_1(\rho, \tau)$. The condition $\overline{G}_1(\rho, \tau = 0)$ represents the classical photon reflectance.

MC simulations have been performed for a wide range of optical parameters and only some representative results have been reported in the Results section.

3. RESULTS

Figure 1 shows a set of $\overline{G}_1(\rho, \tau)$ curves, for different optical parameters, demonstrating the good quality of the proposed analytical approach. All the analytical CTE solutions have been performed for $P_N = 7$. Higher P_N values do not improve the quality of the agreement with the MC reference curves. The largest deviations from MC, appearing for small τ, are always smaller than ~1%. By increasing the number of photon packets in the MC simulation, the deviation between the two methods decreases (not shown), because the precision of the MC method is improved. Unfortunately, this improved calculation takes an unreasonable amount of computation time. In this frame, note that for the condition $\tau = 0$ (also representing the normal RTE solution), and for a larger number of photon packets, the error has already been demonstrated to be of the order of ~1 [16]. Moreover, we must also highlight the fact that the τ dependent $\overline{G}_1(\rho, \tau)$ MC curves are smooth due to the properties of the exact MC algorithm here utilized as proposed in Ref. [11]; in fact, subsequent points are correlated (see Section 2.C). This means that the precision of the first $\overline{G}_1(\rho, \tau)$ point at $\tau = 0$ is a basic condition for the precision of the following points at $\tau > 0$. This also explains why we have no "noise" along the τ dimension. It is interesting to note the reliability of the simulations for the nondiffusive domain (i.e., $\rho \approx 1$ mm). Other simulations performed for other sets of parameters (not shown) always display a similar good quality.

All the simulations shown in Fig. 1 are for the case $P_{\text{m}} = 1$, with all the scatterers that are moving. This may hold, e.g., for

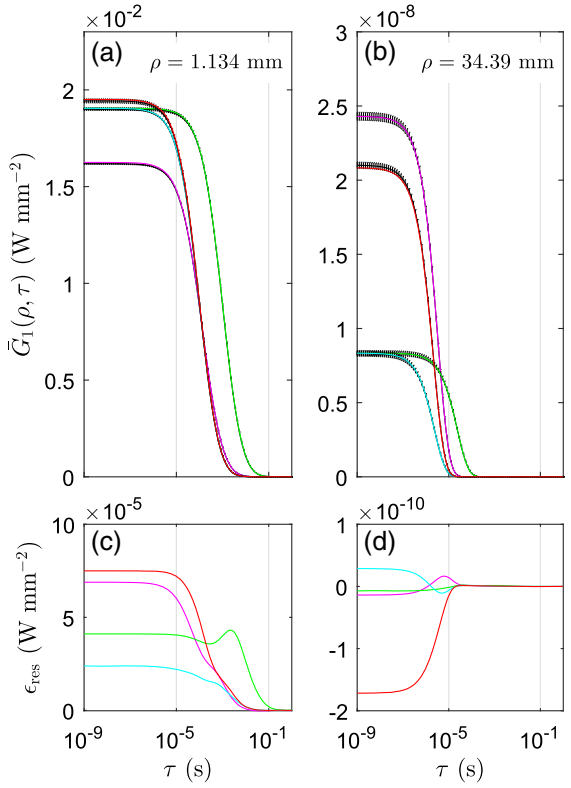

Fig. 1. Panels (a) and (b): analytical CTE solution (**colored**) compared to MC solution (**black**). Common parameters are $n = 1.4$, $g = 0.9$, $\lambda = 785$ nm and $P_{\text{m}} = 1$. (**red**) $\mu'_s = 1$ mm^{-1}, $\mu_a = 0.02$ mm^{-1}, and $D_B = 1 \times 10^{-5}$ mm^2 s^{-1}; (**cyan**) $\mu'_s = 1$ mm^{-1}, $\mu_a = 0.025$ mm^{-1}, and $D_B = 1 \times 10^{-5}$ mm^2 s^{-1}; (**green**) $\mu'_s = 1$ mm^{-1}, $\mu_a = 0.025$ mm^{-1}, and $D_B = 1 \times 10^{-6}$ mm^2 s^{-1}; (**magenta**) $\mu'_s = 0.8$ mm^{-1}, $\mu_a = 0.025$ mm^{-1}, and $D_B = 1 \times 10^{-5}$ mm^2 s^{-1}. Panels (c) and (d) report the residuals, ϵ_{res} (i.e., the difference between MC and CTE curves), of panels (a) and (b), respectively. Closely packed vertical bars represent standard deviations.

optical phantoms such as microspheres diluted in water. However, $P_{\text{m}} = 1$ cannot represent the majority of the biological tissues. In fact, in biological tissues, only a fraction of the scatterers are moving (mainly red blood cells), i.e., $P_{\text{m}} < 1$. For this reason, in Fig. 2 we have reported some curves showing the influence of varying $P_{\text{m}} < 1$ on $\overline{G}_1(\rho, \tau)$. It clearly appears that when not all the detected photons have interacted with a moving scatterer, the $\overline{G}_1(\rho, \tau)$ does not go to 0 for large τ, while the usual DCS models always go to 0 [4]. In this case, $\overline{G}_1(\rho, \tau)$ reaches a constant value >0. This value is the fraction of the total reflectance $\overline{G}_1(\rho, \tau = 0)$, representing the photons that did not interact with a moving scatterer $(\overline{G}_1(\rho, \tau = +\infty))$. In fact, only the interactions of photons with *moving* scatterers provoke the "decorrelation" of $\overline{G}_1(\rho, \tau)$. This effect decreases with increasing ρ, because increasing the source–detector spacing also increases the number of photons that have interacted with a moving scatterer before reaching the detector.

4. DISCUSSION AND CONCLUSIONS

It has been demonstrated that a very simple modification [Eq. (11)] of the classical RTE theory/software allows one to

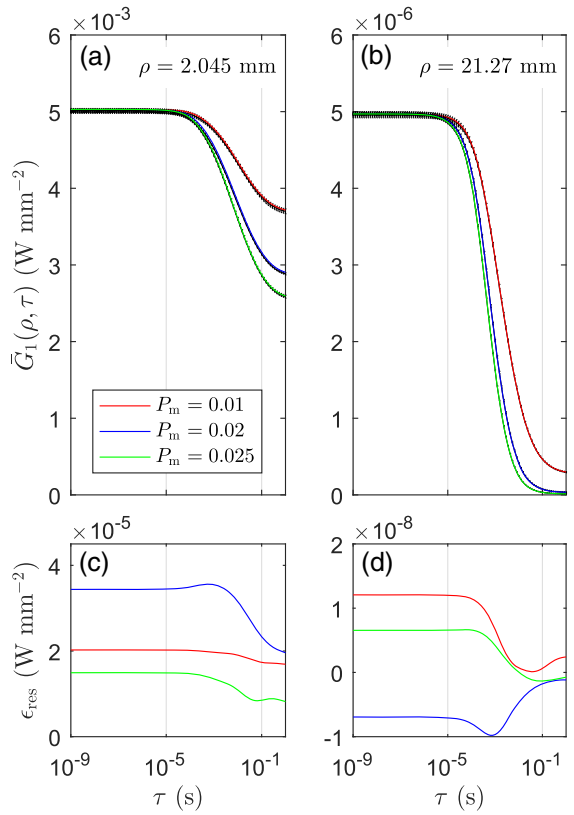

Fig. 2. Panels (a) and (b): analytical CTE solution (**colored**) compared to MC solution (**black**). Common parameters are $n = 1.4$, $g = 0.9$, $\lambda = 785$ nm, $\mu_s' = 0.5$ mm^{-1}, $\mu_a = 0.025$ mm^{-1}, and $D_B = 1 \times 10^{-5}$ mm^2 s^{-1}. Panels (c) and (d) report the residuals, ϵ_{res} (i.e., the difference between MC and CTE curves), of panels (a) and (b), respectively. Closely packed vertical bars represent standard deviations.

generate the solution of the CTE. The results appear to be reliable and in agreement with "gold standard" MC simulations. To the best of our knowledge, this is the first time that an explicit analytical solution for the CTE is given. In particular, the specific influence of the static background on $\overline{G}_1(\rho, \tau)$, as shown in Fig. 2, has never been described before. Results for $\overline{G}_1(\rho, \tau)$ at small ρ have also probably never been shown. Moreover, even if the improved technique for the "gold standard" MC simulations has been suggested in Ref. [11], its explicit implementation and comparison with analytical data (no analytical solution is proposed in Ref. [11]) have never been published before.

The generated $\overline{G}_1(\rho, \tau)$ noise-free curves are valid over a large range of optical and physiological parameters, and in particular for physical systems that are not in the diffusive regime. This represents a generalization of the DCS theory that may be useful in biomedical optics or other domains of physics where, for technical reasons, the source/detector separation cannot always be large enough to satisfy the diffusion conditions. An exact model at short source/detector separation is also interesting for superficial flow characterization. Moreover, since the CTE has the same analytical "form" of the RTE, the present approach might be used for the 2D/3D reconstruction of blood flow distribution from optical tomography data. In principle, by exploiting the known mathematical techniques for the RTE inverse problem [21] and by using the substitution appearing in Eq. (11), the blood flow distribution can be assessed. It remains to be demonstrated that this approach is numerically stable and solvable in a reasonable amount of computation time. However, this is a matter for future investigations.

From Fig. 1 it is interesting to observe that when going from small ρ [Fig. 1(a)] to large ρ values [Fig. 1(b)], the $\overline{G}_1(\rho, \tau)$ behavior is not trivial. For example, the lowest $\overline{G}_1(\rho, \tau)$ values at small τ in [Fig. 1(a)] become the highest in [Fig. 1(b)] for the same optical parameter values (magenta curves). This is due to the interplay existing between the depth z_0 of the point source and the source/detector separation.

The results in Fig. 2 well describe the behavior of $\overline{G}_1(\rho, \tau)$ when $P_m < 1$. The possibility to work with small P_m is fundamental, e.g., when investigating the blood flow of some particular tissues, such as the human bone, where the blood volume fraction is very low (i.e., small P_m). Figure 2 represents also an example where the theoretical conditions for the validity of the DCS model are not satisfied. In fact, the varying part of $\overline{G}_1(\rho, \tau)$ is situated at τ values larger than the critical $\tau_c = (2D_B(2\pi n/\lambda)^2)^{-1} \approx 4 \times 10^{-4}$ value, where the DCS diffusion approximation in principle does not work [10]. Thus, the present approach may be useful for the study of such particular cases, and for the test of the classical approximated algorithms allowing the extraction of blood flow parameters from autocorrelation functions.

It is worth noting that by modifying $g_{1,\text{single}}(\hat{\Omega} \cdot \hat{\Omega}', \tau)$, the proposed approach may be applied to other particle speed distributions. A different geometry of the medium (e.g., slab) and light source type (e.g., Gaussian beam normal or oblique to the surface) can also be easily considered.

In conclusion, we hope that the present approach will help the DCS community to investigate new ways in particle movement monitoring.

REFERENCES

1. R. Dougherty, B. Ackerson, N. Reguigui, F. Dorri-Nowkoorani, and U. Nobbmann, "Correlation transfer: development and application," J. Quant. Spectrosc. Radiat. Transfer **52**, 713–727 (1994).
2. B. Ackerson, R. Dougherty, N. Reguigui, and U. Nobbmann, "Correlation transfer—application of radiative-transfer solution methods to photon-correlation problems," J. Thermophys. Heat Transfer **6**, 577–588 (1992).
3. D. A. Boas, L. E. Campbell, and A. G. Yodh, "Scattering and imaging with diffusing temporal field correlations," Phys. Rev. Lett. **75**, 1855–1858 (1995).
4. T. Durduran, R. Choe, W. B. Baker, and A. G. Yodh, "Diffuse optics for tissue monitoring and tomography," Rep. Prog. Phys. **73**, 076701 (2010).
5. M. Ninck, M. Untenberger, and T. Gisler, "Diffusing-wave spectroscopy with dynamic contrast variation: disentangling the effects of blood flow and extravascular tissue shearing on signals from deep tissue," Biomed. Opt. Express **1**, 1502–1513 (2010).
6. M. Diop, K. Verdecchia, T.-Y. Lee, and K. S. Lawrence, "Calibration of diffuse correlation spectroscopy with a time-resolved near-infrared technique to yield absolute cerebral blood flow measurements," Biomed. Opt. Express **2**, 2068–2081 (2011).
7. I. Bigio and S. Fantini, *Quantitative Biomedical Optics: Theory, Methods, and Applications*, Cambridge Texts in Biomedical Engineering (Cambridge University, 2016).

8. T. Binzoni and F. Martelli, "Assessing the reliability of diffuse correlation spectroscopy models on noise-free analytical Monte Carlo data," Appl. Opt. **54**, 5320–5326 (2015).
9. T. Binzoni, B. Sanguinetti, D. Van de Ville, H. Zbinden, and F. Martelli, "Probability density function of the electric field in diffuse correlation spectroscopy of human bone *in vivo*," Appl. Opt. **55**, 757–762 (2016).
10. D. A. Boas, "Diffuse photon probes of structural and dynamical properties of turbid media: theory and biomedical applications," Ph. D. dissertation (University of Pennsylvania, 1996).
11. R. Pierrat, "Transport equation for the time correlation function of scattered field in dynamic turbid media," J. Opt. Soc. Am. A **25**, 2840–2845 (2008).
12. L. G. Henyey and J. L. Greenstein, "Diffuse radiation in the Galaxy," Astrophys. J. **93**, 70–83 (1941).
13. V. Markel, "Modified spherical harmonics method for solving the radiative transport equation," Waves Random Media **14**, L13–L19 (2004).
14. G. Panasyuk, J. Schotland, and V. Markel, "Radiative transport equation in rotated reference frames," J. Phys. A **39**, 115–137 (2006).
15. M. Machida, G. Y. Panasyuk, J. C. Schotland, and V. A. Markel, "The Green's function for the radiative transport equation in the slab geometry," J. Phys. A **43**, 065402 (2010).
16. A. Liemert and A. Kienle, "Light transport in three-dimensional semi-infinite scattering media," J. Opt. Soc. Am. A **29**, 1475–1481 (2012).
17. A. Liemert and A. Kienle, "Green's function of the time-dependent radiative transport equation in terms of rotated spherical harmonics," Phys. Rev. E **86**, 036603 (2012).
18. D. J. Pine, D. A. Weitz, P. M. Chaikin, and E. Herbolzheimer, "Diffusing wave spectroscopy," Phys. Rev. Lett. **60**, 1134–1137 (1988).
19. P.-A. Lemieux, M. U. Vera, and D. J. Durian, "Diffusing-light spectroscopies beyond the diffusion limit: The role of ballistic transport and anisotropic scattering," Phys. Rev. E **57**, 4498–4515 (1998).
20. R. Carminati, R. Elaloufi, and J.-J. Greffet, "Beyond the diffusing-wave spectroscopy model for the temporal fluctuations of scattered light," Phys. Rev. Lett. **92**, 213903 (2004).
21. S. R. Arridge and J. C. Schotland, "Optical tomography: forward and inverse problems," Inverse Probl. **25**, 123010 (2009).